

Water Splitting

Development of an O₂-Sensitive Fluorescence-Quenching Assay for the Combinatorial Discovery of Electrocatalysts for Water Oxidation**

James B. Gerken,* Jamie Y. C. Chen, Robert C. Massé, Adam B. Powell, and Shannon S. Stahl*

Electrochemical water oxidation is a major focus of solar energy conversion efforts. This anodic half-reaction affords electrons and protons needed to achieve fuel production by reduction of water, CO₂, or other abundant feedstocks at the cathode of a photoelectrochemical cell (PEC; Figure 1).^[1–3]

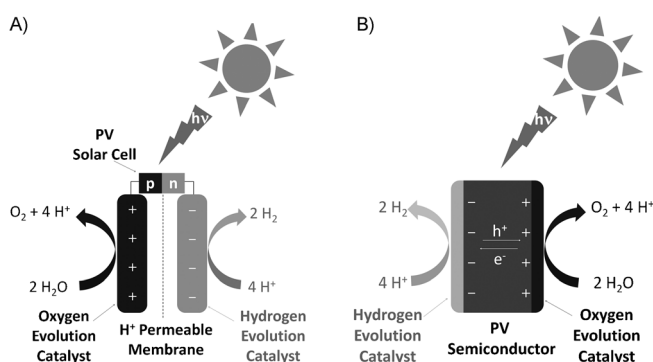


Figure 1. Schematic representations of indirect (A) and direct (B) PEC configurations for water splitting. The former employs a PV solar cell coupled to an electrolysis cell, whereas the latter features direct integration of the electrocatalysts with the charge-separating PV semiconductor.

High kinetic barriers associated with the oxidation of water to O₂^[4,5] and the common use of high-cost electrocatalytic materials are among the challenges that limit the utility of photoelectrochemical energy storage. Improved electrocatalysts that operate at lower overpotential and avoid the use of expensive precious-metal or rare-earth elements are needed. While valuable progress is being made toward this goal,^[1,4–10]

the rational design of optimal catalysts from first principles remains infeasible, and the number of possible catalyst compositions, even those with well-defined metal stoichiometry, far exceeds the number that can be tested in a traditional sequential fashion. Combinatorial methods can play an important role in the discovery of new electrocatalysts, and we describe herein a fluorescence-based assay for spatially resolved, direct detection of O₂ across an array of metal-oxide electrocatalysts. Initial implementation of this technique has led to the identification of new electrocatalysts, which are composed entirely of earth-abundant elements (e.g., Ni/Al/Fe) and warrant further investigation.

Combinatorial methods for the discovery of electrocatalysts have been pursued previously. For example, a soluble fluorescent pH indicator has been used to screen electrocatalysts for reactions that consume or generate protons,^[11] including water oxidation mediated by platinum-group-metal electrocatalysts.^[12] Potential complications with this method include the use of poorly buffered electrolytes to ensure sensitivity to pH changes, and the instability of organic pH-sensitive fluorophores under conditions required for water oxidation. Various combinatorial approaches have been used to probe photoelectrocatalytic performance of mixed-metal-oxide materials. In most of these assays, the oxides are required to act simultaneously as a light-harvesting semiconductor and as the electrocatalyst for one or both water-splitting half-reactions.^[13–18] The most efficient PECs, however, will probably integrate separate photovoltaic (PV) and catalytic materials.^[19–22] Therefore, we targeted an assay that would enable rapid assessment of electrocatalysts for water oxidation independent of the other PEC functions. Catalysts discovered by such methods could then be used in indirect PECs (Figure 1 A) or developed further for integration with PV semiconductors in direct PECs (Figure 1 B).

The essential feature of electrocatalytic water oxidation is O₂ production, and an ideal catalyst-screening assay would directly monitor O₂ evolution. In addition, a fluorescence-based assay seemed appealing because such methods are often compatible with parallel, rather than serial, analysis of activity, and they avoid the need for costly specialized analytical instrumentation. Fluorescent pressure-sensitive paints are well suited to meet these criteria. These paints are used in the automobile and aerospace industries to study aerodynamics in wind tunnels, and their utility arises from the sensitivity of their fluorescence intensity to the partial pressure of O₂ (pO₂).^[23] Quantitative measurements are improved by incorporating two fluorophores into the paint, one that is insensitive to O₂ as a background reference, and another that exhibits fluorescence quenching in proportion to the pO₂. Our assay takes advantage of a commercially

[*] Dr. J. B. Gerken, J. Y. C. Chen, R. C. Massé, Dr. A. B. Powell, Prof. S. S. Stahl
Department of Chemistry, University of Wisconsin-Madison
1101 University Avenue, Madison, WI 53706 (USA)
E-mail: jbergerken@chem.wisc.edu
stahl@chem.wisc.edu
Homepage: <http://www.chem.wisc.edu/~stahl>

[**] We are grateful to Profs. Daniel C. Fredrickson and Robert J. McMahon (UW-Madison), who shared valuable equipment for this project. We thank Profs. Bruce Parkinson (Wyoming) and Jennifer Schuttlefield (UW-Oshkosh) for illuminating discussions and Jerry Stann and Tracy Drier (UW-Madison) for assistance with construction of the apparatus. Jonathan Gerken (Analog Systems Press) and Prof. Thatcher Root (UW-Madison) provided valuable advice on digital image processing. This research was supported by the NSF CCI grant CHE-0802907.

Supporting information for this article is available on the WWW under <http://dx.doi.org/10.1002/anie.201201999>.

available dual-chromophore paint that exhibits O₂-insensitive green and reversible O₂-sensitive red fluorescence.^[24]

A schematic representation of the electrochemical cell is depicted in Figure 2. The key components are a fluorine-doped tin oxide (FTO) electrode with an array of prospective

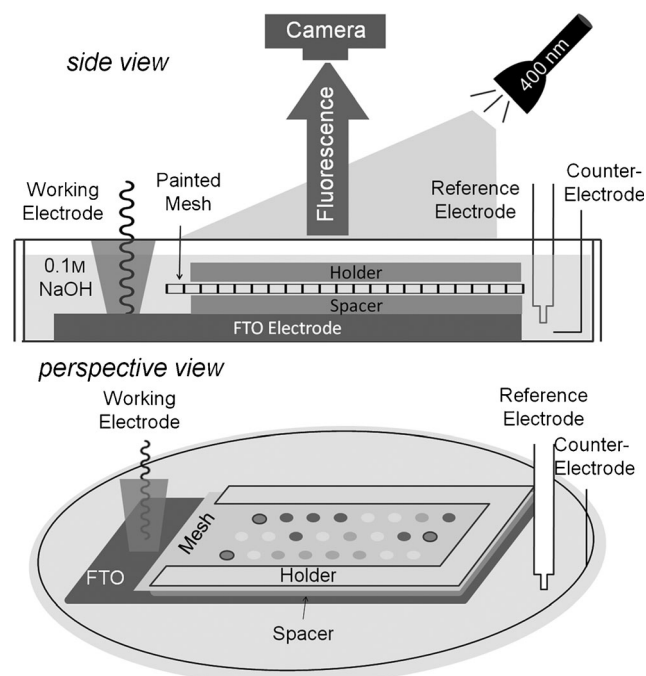


Figure 2. Schematic drawing (side and perspective views) of the electrochemical screening apparatus showing the positions of the electrode array, O₂-sensing mesh, light source, and camera.

metal-oxide electrocatalysts and a stainless steel mesh coated with fluorescent paint. These components are aligned in parallel layers and immersed in the electrolyte (0.1M NaOH). The spacing between the electrode and painted mesh (1 mm) is set to enable good resolution of the fluorescence signal between adjacent catalyst spots. The three-electrode cell is then sealed, purged with Ar, and electrolyzed at 670 mV vs Ag/AgCl [overpotential (η) = 406 mV]. During electrolysis the cell is irradiated at specified time intervals with $\lambda = 400$ nm light, and the green and red fluorescence emanating from the painted mesh is captured by a digital camera. Dissolved oxygen diffuses from the individual catalysts and quenches the red fluorescence signal in proportion to the amount of O₂ evolved. Analysis of the red/green fluorescence intensity ratios at each spot provides the basis for assessment of the water-oxidation activity of individual catalysts.

The selection of prospective electrocatalysts emphasized metals from among the first-row transition series, as they have sufficient terrestrial abundance to be viable in large-scale applications. Mixed oxides of these metals in well-defined stoichiometry (e.g. NiCo₂O₄, etc.) have been investigated previously, as have nonstoichiometric binary and ternary mixed oxides,^[25–30] but the diversity space is far from well explored. Mid-to-late first-row transition metals provide

excellent capacity to access multiple oxidation states, and different redox-active metals in the catalytic material could play synergistic roles in buffering the multielectron processes needed to achieve efficient water oxidation. The role of a Ca²⁺ ion in the oxygen-evolving complex of Photosystem II^[3a,31] raised the possibility that non-redox-active Lewis-acidic metal ions (e.g., Ca²⁺, Mg²⁺, Al³⁺) could enhance catalyst activity, for example, by facilitating deprotonation of a reactive water molecule or formation of the O–O bond. Alternatively, such non-redox-active metal ions could have a beneficial structural role in the oxide material.

Twenty-one different ternary metal-oxide combinations (Table 1) were screened using the fluorescence assay described above. For each triad, solutions of the corresponding

Table 1: List of the mixed-oxide triads investigated in this study.

Metal-ion triads tested		
Co/Al/Fe	Co/La/Ca	Ni/Al/Cr
Co/Al/Ni	Co/Ce/Al	Ni/Ca/Fe
Co/Fe/Ni	Co/La/Al	Ni/Mg/Fe
Co/Fe/Mn	Ni/Al/Fe	Ni/Zn/Fe
Co/Fe/Cr	Ni/Fe/Mn	Ni/Ce/Al
Co/La/Fe	Ni/Fe/Cr	Ni/La/Al
Co/Ce/Fe	Ni/Ce/Fe	Ni/La/Fe

metal salts were mixed in stoichiometries of M¹_(100%–x)/M²_(x–y)/M³_y, with x and y varied in increments of 20% from 0 to 100%, so as to sample across the ternary composition diagram (Figure 3A). These mixtures were then arrayed onto an FTO-coated glass electrode (Figure 3B) and calcined

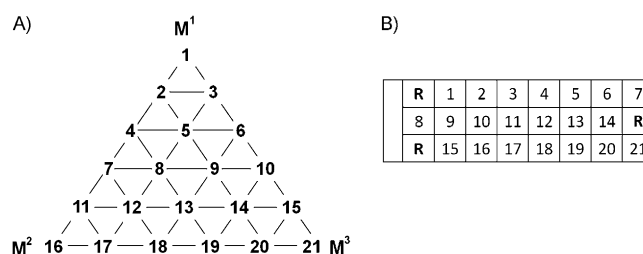


Figure 3. A) Ternary-oxide composition diagram, spot 1 is 100% M¹, spot 5 is 60% M¹, 20% M², 20% M³, etc. B) Arrangement of metal-oxide compositions on the electrode array; R represents reference metal-oxide compositions held constant from electrode to electrode.

at 500 °C (see Scheme S1 in the Supporting Information). The arrays were then electrolyzed and assayed for oxygen evolution as described above.

Cobalt and nickel oxides have been widely studied as electrocatalysts for water oxidation,^[4,6,25,32,33] and screening data for the Co/Al/Ni triad illustrates the assay methodology (Figure 4). As catalytic O₂ evolution manifests itself through a quenching of the red fluorescence signal, photographs obtained during electrolysis reveal green spots over some of the electrocatalyst positions (Figure 4A). Image processing enables red and green channels to be separated within the

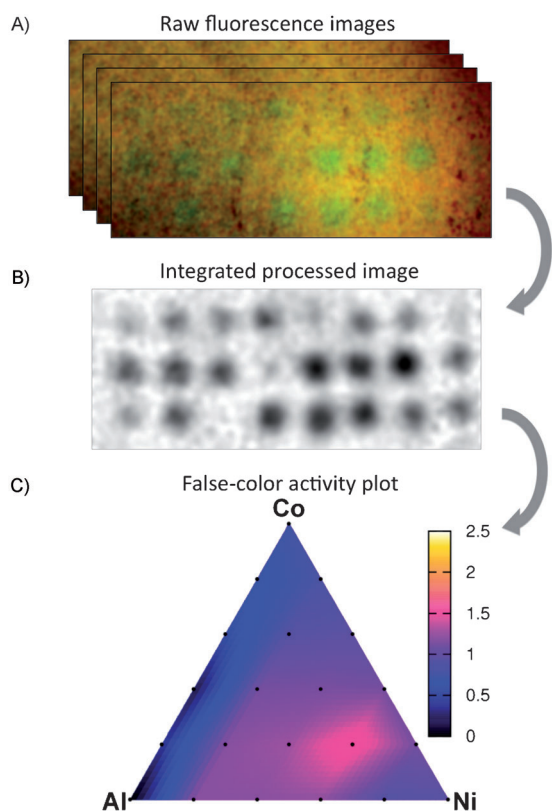


Figure 4. Data-processing sequence for the fluorescence-quenching assay. A) Stacked raw images of the fluorescent grid above a Co/Al/Ni array during electrolysis (contrast-enhanced for clarity). B) Back-ground-subtracted grayscale image of the sum of the red/green processed images from the stack depicted in (A). C) False-color ternary composition diagram of the Co/Al/Ni triad data (average of 3 experiments) showing normalized activities with an optimum at $\text{Co}_{20}\text{Al}_{20}\text{Ni}_{60}\text{O}_x$.

photographs (see the Supporting Information), and the red/green intensity ratios from each photograph were summed and background corrected to create a single grayscale image in which the integrated spot intensities correlate with the amount of O_2 produced from individual electrocatalysts (Figure 4B, and Scheme S2 in the Supporting Information).^[34] These intensities were normalized with respect to reference spots in the array and plotted as a false-color map on a ternary composition diagram for the triad (Figure 4C). A noteworthy result from the Co/Al/Ni triad data is the effect of the redox-inert, Lewis-acidic Al^{3+} on electrocatalytic activity. The $\text{Co}_{20}\text{Al}_{20}\text{Ni}_{60}\text{O}_x$ oxide composition exhibits higher activity than the monometallic Co and Ni oxides, as well as Co/Ni binary oxides, which have been used extensively in water electrolysis applications.^[1,4,25,32,33]

Analogous fluorescence-based activity data were acquired for each of the other twenty triads identified in Table 1 (see Figures S4–S24 in the Supporting Information). Most of these compositions have not been reported previously. However, in cases where literature data exists, the relative activities obtained from our screening show good correlation with reported data for the corresponding binary and ternary mixtures. Examples include several compositions

within the Co/Fe/Ni, Co/Fe/Mn, and Co/Fe/Cr triads.^[26,28] From our screening data, the highest electrocatalytic activity was detected from combinations of Ni, Fe, and a redox-inert metal ion, most notably, $\text{Ni}_{60}\text{Al}_{20}\text{Fe}_{20}\text{O}_x$ and $\text{Ni}_{40}\text{Al}_{40}\text{Fe}_{20}\text{O}_x$ (Figure 5). The improved activity observed upon incorporation of Al^{3+} into the Ni/Fe oxide material highlights the

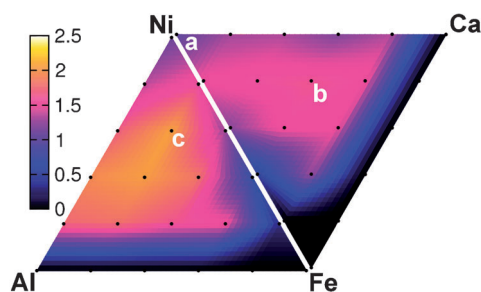


Figure 5. Plot of activity versus composition for the triads Ni/Al/Fe and Ni/Ca/Fe, with labels a, b, and c identifying compositions investigated by steady-state Tafel analysis as shown in Figure 6.

beneficial effect of redox-inert metal ions on the activity of water-oxidation electrocatalysts. These observations are noteworthy in light of a previously reported photoelectrochemical cell having a binary Ni/Fe oxide electrocatalyst, which achieved a solar-to-hydrogen conversion efficiency as high as 7.8%.^[19]

The results of the fluorescence assays were validated by several independent control experiments. The relative activities of different spots in the arrays were reproducible across multiple runs and replicated samples, as revealed by the similar activities of independently tested Ni/Fe binary mixtures from the Ni/Al/Fe and Ni/Ca/Fe triads (see the shared edge from these triads in Figure 5). Fifteen of the 441 oxide compositions tested were selected for further investigation by steady-state Tafel analysis (Figure 6A and Figures S25A–E in the Supporting Information). A close correlation was observed between the relative catalytic activities obtained from the fluorescence assay and those from the steady-state current densities at a constant overpotential from the Tafel analysis (Figure 6B).^[35] These data show that the newly discovered $\text{Ni}_{60}\text{Al}_{20}\text{Fe}_{20}\text{O}_x$ catalyst exhibits an overpotential (η) 135 mV lower than that of a cobalt oxide catalyst at a current density of 10 mA cm^{-2} (Figure S25C). Tafel data for the latter cobalt oxide sample closely matched those from a cobalt oxide film prepared by electrodeposition, when normalized for electrochemically active surface area (Figure S28).^[10e,36] Finally, a bulk electrode (15 cm^2) coated with the $\text{Ni}_{60}\text{Al}_{20}\text{Fe}_{20}\text{O}_x$ catalyst, exhibited a 99% Faradaic yield of O_2 (Figure S29). Overall, these results clearly demonstrate that the fluorescence-based data are an excellent predictor of electrocatalyst performance.

The results of this electrochemical assay can be compared to previous photoelectrochemical screening studies wherein similar metal-oxide materials served as a photovoltaic semiconductor and as an electrocatalyst. Oxide compositions within the Co/Al/Fe triad exhibited only cathodic activity in a photoelectrochemical screen,^[14] but they show respectable

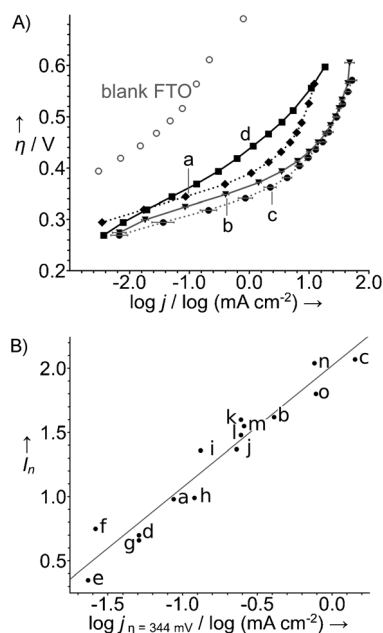


Figure 6. A) Tafel current/polarization data for selected catalyst compositions identified via fluorescence-quenching assays. X-axis error bars reflect one standard deviation based on multiple samples. B) Correlation of catalyst activity derived from the fluorescence-quenching and steady-state Tafel data (I_n is the dimensionless ratio $R \cdot G_{\text{ref}} / R_{\text{ref}} \cdot G^{-1}$ where R and G are the red and green intensities of the catalyst or reference; linear fit $R^2 = 0.94$. See the Supporting Information for the choice of abscissa). Estimated errors: 0.16 (I_n) and 0.10 ($\log j$). Compositions tested: a: Ni_{100} , b: $\text{Ni}_{40}\text{Ca}_{40}\text{Fe}_{20}$, c: $\text{Ni}_{60}\text{Al}_{20}\text{Fe}_{20}$, d: Co_{100} , e: $\text{Co}_{40}\text{Fe}_{40}\text{Cr}_{20}$, f: $\text{Co}_{40}\text{Fe}_{20}\text{Mn}_{40}$, g: $\text{Co}_{20}\text{Fe}_{40}\text{Mn}_{40}$, h: $\text{Co}_{20}\text{Fe}_{20}\text{Cr}_{60}$, i: $\text{Co}_{20}\text{Fe}_{20}\text{Ni}_{60}$, j: $\text{Co}_{60}\text{Al}_{20}\text{Fe}_{20}$, k: $\text{Co}_{20}\text{Al}_{20}\text{Ni}_{60}$, l: $\text{Co}_{60}\text{Al}_{20}\text{Fe}_{20}$, m: $\text{Ni}_{20}\text{Ca}_{60}\text{Fe}_{20}$, n: $\text{Ni}_{40}\text{Al}_{40}\text{Fe}_{20}$, o: $\text{Ni}_{20}\text{Al}_{60}\text{Fe}_{20}$.

oxygen-evolving activity in the present screen (see Figure S4 in the Supporting Information). Observations such as these underscore the value of directly measuring the property that one wishes to optimize through screening because good photoanode materials are not necessarily good catalysts for water oxidation and vice versa.

The data acquired in this initial work suggest redox-inert Lewis-acidic metal ions can be effective promoters of electrocatalytic activity of mixed-metal oxides, possibly resembling the role of Ca^{2+} in biological oxygen evolution.^[3a,31] Earth-abundant Lewis-acidic metal ions, such as Al^{3+} , represent appealing, economical alternatives to La^{3+} and other rare-earth elements commonly featured in heterogeneous catalysts for water oxidation.^[1,7]

Additional work will be needed to elucidate the mechanistic roles of constituent cations, characterize the structure and morphology of specific catalyst compositions, and determine long-term catalyst stability. Nevertheless, the results presented here highlight an efficient and effective fluorescence-based assay for discovery of new oxygen-evolving electrocatalysts. Primary screening methods of this type are critical to the identification of catalytic materials worthy of more-systematic investigation and optimization for the development of practical and efficient multimeral photoelectrochemical solar energy storage devices.

Received: March 13, 2012
Published online: May 24, 2012

Keywords: electrochemistry · heterogeneous catalysis · high-throughput screening · transition metals · water splitting

- a) M. G. Walter, E. L. Warren, J. R. McKone, S. W. Boettcher, Q. X. Mi, E. A. Santori, N. S. Lewis, *Chem. Rev.* **2010**, *110*, 6446–6473; b) P. Du, R. Eisenberg, *Energy Environ. Sci.* **2012**, *5*, 6012–6021.
- M. Grätzel, *Nature* **2001**, *414*, 338–344.
- a) G. F. Moore, G. W. Brudvig, *Annu. Rev. Condens. Matter Phys.* **2011**, *2*, 303–327; b) R. E. Blankenship et al., *Science* **2011**, *332*, 805–809, see Supp. Info.; c) H. Michel, *Angew. Chem.* **2012**, *124*, 2566–2568; *Angew. Chem. Int. Ed.* **2012**, *51*, 2516–2518.
- H. Dau, C. Limberg, T. Reier, M. Risch, S. Roggan, P. Strasser, *ChemCatChem* **2010**, *2*, 724–761.
- T. A. Betley, Q. Wu, T. Van Voorhis, D. G. Nocera, *Inorg. Chem.* **2008**, *47*, 1849–1861.
- M. W. Kanan, Y. Surendranath, D. G. Nocera, *Chem. Soc. Rev.* **2009**, *38*, 109–114.
- J. O'M. Bockris, T. Otagawa, *J. Electrochem. Soc.* **1984**, *131*, 290–302.
- J. Suntivich, K. J. May, H. A. Gasteiger, J. B. Goodenough, Y. Shao-Horn, *Science* **2011**, *334*, 1383–1385.
- a) A. J. Esswein, M. J. McMurdo, P. N. Ross, A. T. Bell, T. D. Tilley, *J. Phys. Chem. C* **2009**, *113*, 15068–15072; b) F. Jiao, H. Frei, *Angew. Chem.* **2009**, *121*, 1873–1876; *Angew. Chem. Int. Ed.* **2009**, *48*, 1841–1844; c) F. Jiao, H. Frei, *Chem. Commun.* **2010**, *46*, 2920–2922; d) B. S. Yeo, A. T. Bell, *J. Am. Chem. Soc.* **2011**, *133*, 5587–5593.
- a) M. W. Kanan, D. G. Nocera, *Science* **2008**, *321*, 1072–1075; b) Y. Surendranath, M. Dincă, D. G. Nocera, *J. Am. Chem. Soc.* **2009**, *131*, 2615–2620; c) Y. Gorlin, T. F. Jaramillo, *J. Am. Chem. Soc.* **2010**, *132*, 13612–13614; d) J. B. Gerken, E. C. Landis, R. J. Hamers, S. S. Stahl, *ChemSusChem* **2010**, *3*, 1176–1179; e) J. B. Gerken, J. G. McAlpin, J. Y. C. Chen, M. L. Rigsby, W. H. Casey, R. D. Britt, S. S. Stahl, *J. Am. Chem. Soc.* **2011**, *133*, 14431–14442; f) M. Risch, K. Klingan, F. Ringleb, P. Chernev, I. Zaharieva, A. Fischer, H. Dau, *ChemSusChem* **2012**, *5*, 542–549.
- E. Reddington, A. Sapientza, B. Gurau, R. Viswanathan, S. Sarangapani, E. S. Smotkin, T. E. Mallouk, *Science* **1998**, *280*, 1735–1737.
- A. G. Dokoutchaev, F. Abdelrazzaq, M. E. Thompson, J. Willson, C. Chang, A. Bocarsly, *Chem. Mater.* **2002**, *14*, 3343–3348.
- M. Woodhouse, B. A. Parkinson, *Chem. Soc. Rev.* **2009**, *38*, 197–210.
- M. Woodhouse, G. S. Herman, B. A. Parkinson, *Chem. Mater.* **2005**, *17*, 4318–4324.
- J. E. Katz, T. R. Gingrich, E. A. Santori, N. S. Lewis, *Energy Environ. Sci.* **2009**, *2*, 103–112.
- G. R. Winkler, J. R. Winkler, *Rev. Sci. Instrum.* **2011**, *82*, 114101.
- H. Ye, H. S. Park, A. J. Bard, *J. Phys. Chem. C* **2011**, *115*, 12464–12470.
- T. F. Jaramillo, S. H. Baeck, A. Kleiman-Shwarscstein, K.-S. Choi, G. D. Stucky, E. W. McFarland, *J. Comb. Chem.* **2005**, *7*, 264–271.
- R. E. Rocheleau, E. L. Miller, A. Misra, *Energy Fuels* **1998**, *12*, 3–10.
- S. Y. Reece, J. A. Hamel, K. Sung, T. D. Jarvi, A. J. Esswein, J. J. H. Pijpers, D. G. Nocera, *Science* **2011**, *334*, 645–648.
- E. M. P. Steinmiller, K.-S. Choi, *Proc. Natl. Acad. Sci. USA* **2009**, *106*, 20633–20636.
- D. K. Zhong, M. Cornuz, K. Sivula, M. Graetzel, D. R. Gamelin, *Energy Environ. Sci.* **2011**, *4*, 1759–1764.

- [23] a) T. Liu, B. T. Campbell, S. P. Burns, J. P. Sullivan, *Appl. Mech. Rev.* **1997**, *50*, 227–246; b) M. Schäferling, *Angew. Chem. Int. Ed.* **2012**, *51*, 3532–3554; *Angew. Chem.* **2012**, *124*, 3590–3614.
- [24] The molecular identities of the fluorophores are not provided by the vendor, but see Refs. [23a,b] and the Supporting Information for more information.
- [25] Y. Matsumoto, E. Sato, *Mater. Chem. Phys.* **1986**, *14*, 397–426.
- [26] M. I. Godinho, M. A. Catarino, M. I. d. Pereira, M. H. Mendonça, F. M. Costa, *Electrochim. Acta* **2002**, *47*, 4307–4314.
- [27] a) R. N. Singh, J. P. Singh, H. N. Cong, P. Chartier, *Int. J. Hydrogen Energy* **2006**, *31*, 1372–1378; b) M. Kumar, R. Awasthi, A. S. K. Sinha, R. N. Singh, *Int. J. Hydrogen Energy* **2011**, *36*, 8831–8838; c) M. Kumar, R. Awasthi, A. K. Pramanick, R. N. Singh, *Int. J. Hydrogen Energy* **2011**, *36*, 12698–12705.
- [28] R. N. Singh, N. K. Singh, J. P. Singh, *Electrochim. Acta* **2002**, *47*, 3873–3879.
- [29] a) D. M. Robinson, Y. B. Go, M. Greenblatt, G. C. Dismukes, *J. Am. Chem. Soc.* **2010**, *132*, 11467–11469; b) R. K. Hocking, R. Brimblecombe, L.-Y. Chang, A. Singh, M. H. Cheah, C. Glover, W. H. Casey, L. Spiccia, *Nat. Chem.* **2011**, *3*, 461–466; c) I. Zaharieva, M. M. Najafpour, M. Wiechen, M. Haumann, P. Kurz, H. Dau, *Energy Environ. Sci.* **2011**, *4*, 2400–2408.
- [30] a) T.-C. Wen, H.-M. Kang, *Electrochim. Acta* **1998**, *43*, 1729–1745; b) A. Kahoul, A. Hammouche, G. Poillerat, R. W. De Doncker, *Catal. Today* **2004**, *89*, 287–291.
- [31] Y. Umena, K. Kawakami, J.-R. Shen, N. Kamiya, *Nature* **2011**, *473*, 55–60.
- [32] Y.-W. D. Chen, R. N. Noufi, *J. Electrochem. Soc.* **1984**, *131*, 1447–1451.
- [33] M. Dincă, Y. Surendranath, D. G. Nocera, *Proc. Natl. Acad. Sci. USA* **2010**, *107*, 10337–10341.
- [34] R. J. Meier, S. Schreml, X.-d. Wang, M. Landthaler, P. Babilas, O. S. Wolfbeis, *Angew. Chem.* **2011**, *123*, 11085–11088; *Angew. Chem. Int. Ed.* **2011**, *50*, 10893–10896.
- [35] Current densities are reported in terms of the projected area of the catalyst. For relative electrochemically active surface areas, see the Supporting Information.
- [36] Electrodeposited Co oxide exhibits substantially higher surface area than the calcined sample. However, the normalized activities of these samples are very similar. See Figures S26–S28 in the Supporting Information for details.